Polskie Towarzystwo Materiałów Kompozytowych
Polish Society of Composite Materials

25: 3 (2025) 200–208

COMPOSITES THEORY AND PRACTICE

ISSN (online): 2299-128X

Paweł Stabla * (0000-0001-6891-582X), Konrad Kamiński , Łukasz Wacławek , Karolina Paczkowska (0009-0007-4170-3406), Zuzanna Pacholec (0009-0002-4384-0344), Michał Barcikowski (0000-0001-5135-7892), Wojciech Błażejewski (0000-0001-9260-1388)

Wrocław University of Science and Technology, Faculty of Mechanical Engineering, 50-370 Wrocław, Poland
* *Correspondence:* pawel.stabla@pwr.edu.pl

Received (Otrzymano) 15.07.2025
Published on-line (Opublikowano) 30.09.2025

MECHANICAL BEHAVIOUR OF FILAMENT-WOUND GFRP AND BFRP COMPOSITE TUBES

https://doi.org/10.62753/ctp.2025.06.3.3

Composite materials play a crucial role in the development of lightweight and innovative industry. For high-performance structures such as composite pressure vessels, tubes and pipelines, filament-winding technology is used as a highly automated and reliable manufacturing method. In this study, the mechanical investigation of composite tubes is performed. The analysis consists of a comparison of basalt and glass fibre reinforced plastics (BFRP and GFRP) under axial compression loading. The tubes were manufactured with one layer wound using a 55° winding angle and additional hoop reinforcement in the gripping area. During axial compression loading, the acoustic emission method was used to identify the damage modes occurring in the two groups of materials. Post-failure observations were conducted to assess the crack type and geometry. The results showed that GFRP exhibited superior performance over BFRP in terms of compressive strength (41% higher) and absorbed energy (20% higher).

Keywords: filament winding, axial compression, mechanical analysis, BFRP, GFRP, acoustic emission

INTRODUCTION

Composite materials play an important role in modern engineering due to their exceptional strength-to-weight ratio, design possibilities and corrosion resistance. These materials are widely used in aerospace, automotive, civil engineering and marine applications [1–4]. The rapid development of composites has enabled the production of lightweight and highly durable elements. It contributes to energy efficiency, decreases material consumption and enhances mechanical performance.

Among the several composite manufacturing technologies, the filament winding method stands out for its ability to create high-strength, lightweight cylindrical, and even more complicated structures. This method, highly automated (comparing to other composite manufacturing techniques) ensures precise fibre placement and alignment, leading to superior mechanical properties. Filament winding is commonly employed to produce pipes, pressure vessels, rocket motor casting, and wind turbine components, where structural integrity under very demanding conditions is crucial. By using materials such as carbon, glass or basalt fibres, engineers and scientists can tailor composites to meet specific performance requirements. The selection of reinforcement fibres is critical as it directly influences the mechanical properties, durability and overall performance of the resulting composites [5–8].

Glass fibre-reinforced polymer (GFRP) composites have a long-established history in structural applications because of their balance between cost-effectiveness and robust mechanical properties. Recent research aimed at optimizing the filament winding process for glass fibre-reinforced composites has demonstrated improved fibre alignment, a reduced void content, and enhanced structural integrity [9]. Moreover, an evaluation of different reinforcement options has underscored that while glass fibres offer substantial benefits, basalt fibres provide an emerging alternative with unique attributes. For example, studies comparing glass and basalt fibre reinforcements indicate that basalt fibres can yield comparable or even superior performance under specific environmental and thermal conditions [10].

Basalt fibres, which are produced from natural volcanic rock, have garnered increasing interest owing to their excellent thermal stability, chemical resistance, and favourable mechanical characteristics. Research on basalt fibre composites shows that they can offer higher tensile strength and improved durability when compared to conventional glass fibre composites [11, 12]. The thermal and mechanical behaviour of both glass and basalt fibre composites has been studied extensively, demonstrating that the integration of these fibres results in materials well-suited for harsh environments [13].

Recognizing the complementary properties of glass and basalt fibres, recent studies have explored hybrid composite systems. By combining the cost-effective, high-strength properties of glass fibres with the superior thermal and chemical stability of basalt fibres, researchers have developed hybrid composites that are tailored to meet specific performance demands. For instance, mechanical characterizations of such hybrid systems indicate a marked improvement in durability and impact resistance as the synergistic effects of the two fibres result in a composite that outperforms systems made from a single type of reinforcement [14, 15]. The environmental effects on fibre-reinforced polymers have also been addressed, with findings suggesting that optimized material selection and process control can significantly mitigate degradation resulting from hydrothermal aging and chemical exposure [16].

The presented study fills the gap of direct comparison and analysis of GFRP and BFRP filament-wound tubes. In the work, axial compression was chosen to compare the mechanical behaviour of the composite structures. The study is supported by the analysis of damage modes occurring in the specimens by means of the acoustic emission method [17–23].

MATERIALS AND METHODS

The materials used in the presented research are glass fibre E-glass and basalt fibre. The matrix was compounded by Araldite LY1564 epoxy resin with Aradur 3474 hardener.

The filament winding process was performed on an MAW 20 LS4/1 filament winder provided by the Mikrosam company. The mandrels were chrome-coated steel rods. To facilitate the winding of helical layers, additional equipment was used, namely, pin rings on both sides of the mandrel. They reduce the turn-around zone and therefore material consumption during the process. The mandrel was cleaned with acetone, wax was applied and polished 3 times, then the process started. One layer of composite was wound on the mandrel with a 55° winding angle. The angle choice was dictated by the literature review as it is the most common angle for filament wound tubes and pipes [24–31]. After winding, shrink tape was applied on the composite to provide proper compaction of the composite and to remove excessive resin before curing. The composites were then solidified in rotational movement, and after a few days removed from the mandrels, and cut into specified dimensions. The last step was to produce the additional hoop reinforcement at the ends of the specimens to enhance the load distribution during the axial compression test. Exemplary photos are presented in Figure 1.

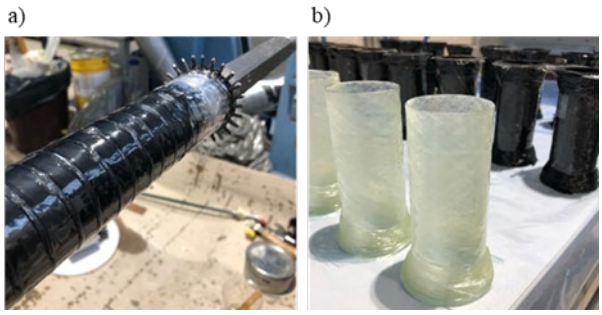

Fig. 1. Filament winding of composite tubes (a), and application of additional hoop reinforcement at ends of specimens (b)

Before incorporating the additional hoop reinforcement, the specimens were measured in terms of dimensions and mass. The values were then used in the strength calculations to reduce the influence of deviations in specimen dimensions. The results of those measurements are presented in Table 1.

TABLE 1. **Geometric and mass characteristics of composite specimens used in axial compression**

Specimen	Mass (g)	Diameter (mm)	Length (mm)
G55-1	23.34	41.91	99.43
G55-2	23.30	41.94	99.53
G55-3	24.02	41.93	99.37
G55-4	23.07	41.85	98.92
G55-5	23.68	41.94	99.60
G55-6	23.54	41.87	98.73
G55-7	23.94	41.91	99.03
G55-8	23.70	41.86	99.43
B55-1	23.18	41.73	99.37
B55-2	23.23	41.89	99.07
B55-3	22.77	41.93	99.60
B55-4	23.62	42.03	99.16
B55-5	23.38	41.86	99.14
B55-6	23.30	41.95	99.46
B55-7	23.65	41.99	99.46
B55-8	23.01	41.99	99.43

After the compete manufacturing process, the specimens were cured in an oven according to the curing process shown in Figure 2.

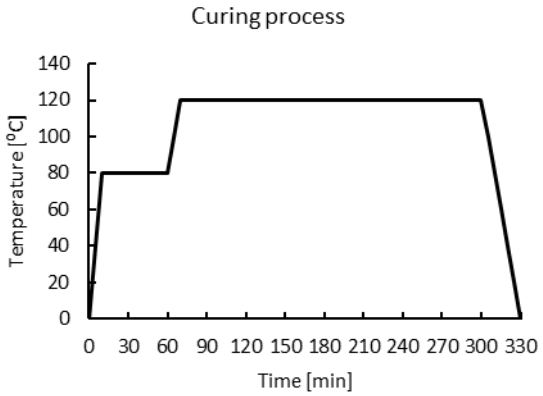

Fig. 2. Curing process of composite tubes

The mechanical test of axial compression was performed on an Instron 5982 universal testing machine with a loading cell of 100 kN. The experimental setup consisted of two platens, where one has a spherical joint. Before the test, the specimens were initially loaded with 50 N force to remove slack from all the force-displacement curves as it is a common procedure described in the literature [32]. The setup with an exemplary specimen is shown in Figure 3.

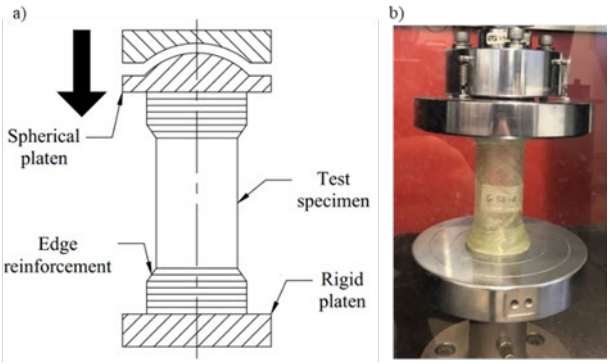

Fig. 3. Diagram of axial compression test (a) and specimen mounted in machine (b)

RESULTS

In this section, the results of the mechanical tests (axial compression), acoustic emissions analysis and macroscopic observations of cracks are presented.

AXIAL COMPRESSION TESTING

The results of the axial compression tests are presented in Figure 4 and Figure 5 for the GFRP and BFRP tubes, respectively. The graphs show the load-displacement curves. In the case of the GFRP specimens, in the elastic part of the test, up to 1 mm of displacement of the moving platen, very satisfactory repeatability is observed. The tubes then started to undergo damage, which is demonstrated in flattening of the force-displacement curve. Next, rapid failure took place and a loss of stability occurred at around 2 mm of displacement.

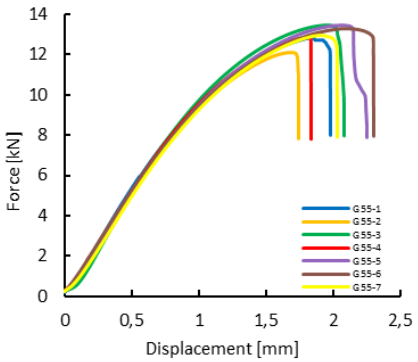

Fig. 4. Force-displacement curves of GFPR tubes subjected to axial compression

In the case of the BFRP samples, greater deviation in the elastic part of the test can be observed. Additionally, the damage was more rapid compared to the GFRP tubes, manifesting in a lesser intensity of flatting of the load-displacement curves. Also, the damage occurred sooner, when the displacement was around 1.5 mm.

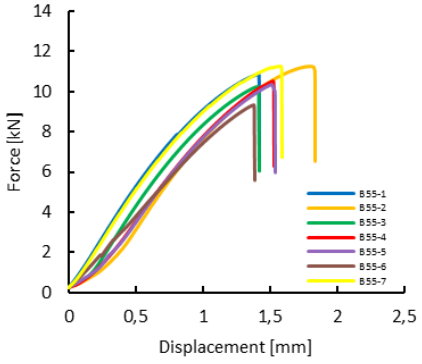

Fig. 5. Force-displacement curves of BFRP tubes subjected to axial compression

To enable a valid comparison between the results of the GFRP and the BFRP configurations, quantitative analysis was performed. As the defining parameter to consider, the compressive strength was calculated following Equation 1:

$$\sigma_c = \frac{F_{max}}{A} \tag{1}$$

Where:
σ – compressive stress [MPa]
A – composite tube cross-section area [mm^2]

The results for both materials are presented in Figure 6.

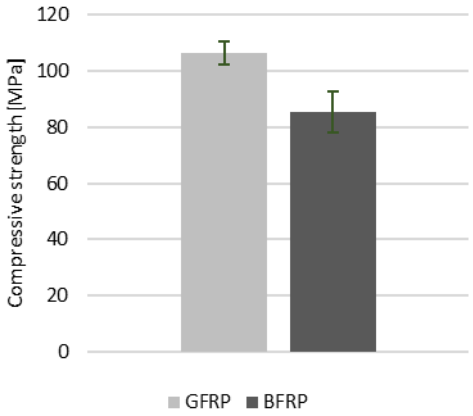

Fig. 6. Compressive strength for GFRP and BFRP specimens

In addition to the compressive strength, the corrected absorbed energy was defined. The absorbed energy is calculated as an area below the force-displacement curve following Equation 2:

$$\Delta E = \int_0^s F \cdot ds \tag{2}$$

Where:
s – displacement [m]
F – compressive force[N]

To reduce the influence of specimen thickness variation, the absorbed energy was divided by the mass of the specific specimen, as presented in Equation 3:

$$E_c = \frac{\Delta E}{m} \tag{3}$$

Where:
Ec – corrected energy [J/kg]
m – specimen mass [kg]

The results showing the differences in corrected absorbed energy are presented in Figure 7.

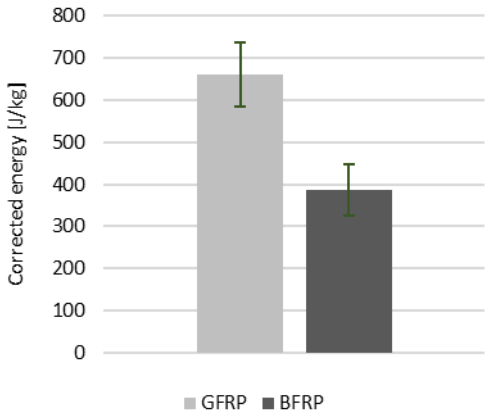

Fig. 7. Corrected absorbed energy for GFRP and BFRP specimens

ACOUSTIC EMISSION RESULTS

Acoustic emission analysis was conducted using a Vallen AMYS-6 (Vallen Systeme, Germany). In the analysis of the acoustic activity of the specimens during the tests, the peak amplitude was chosen as the defining parameter following the literature approaches [33–35].

The acoustic events were divided into three categories regarding the type of damage. The types are typical ones for composite structures and may be defined by the amplitude, according the ranges presented in Table 2.

TABLE 2. **AE parameters ranges for different failure modes**

Failure mode	Amplitude [dB]
M1 – matrix cracking	45-55
M2 – debonding/delamination	55-70
M3 – fibre breakage	70-100

The acoustic events were recorded during axial compression loading , divided according to the failure modes and presented as a division (percent) of the total amount in the GFRP or BFRP specimen. The results are presented in Figure 8.

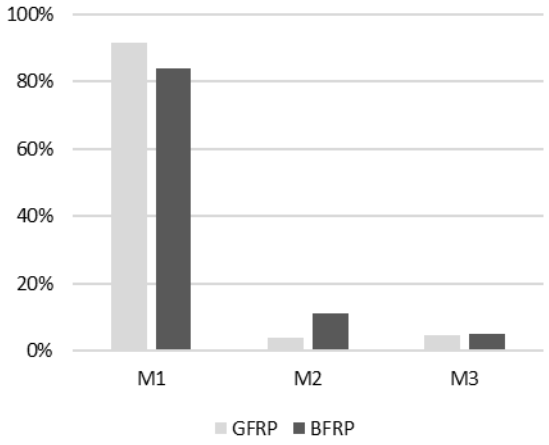

Fig. 8. Acoustic emission results in terms of amplitude of the event regarding different failure modes (M1 – matrix cracking, M2 – debonding/delamination, M3 –- fibre breakage)

MACROSCOPIC EVALUATIONS

The macroscopic observations of the composite tubes enable analysis of the fracture type occurring in each sample and assigning them to groups specific for the type reinforcement used.

Firstly, the GFRP specimens are presented.

V type damage – the fracture of the specimen ran along the wound fibre until the interlace was encountered. At this point, there was a change in the direction of the crack to an angle opposite to the original (initially +55º, finally -55º). The crack was clearly visible on the surface of the specimen, and local irregularities were noticeable in the areas of the change in direction. There was some minor additional damage (folds) in the region of the interlace. The course of this crack may resemble the letter V. An example of a crack is shown in Figure 9.

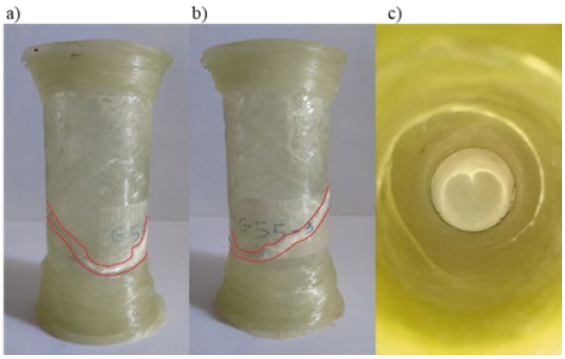

Fig. 9. V type crack in GFRP specimen. Different views of specimen (a and b); internal surface of specimen (c)

C type damage – circumferential fracture – damage to the specimen manifested itself along the entire circumference of the component. The loss of material cohesion occurred differently – along the winding angle, perpendicular to the axis of the specimen as well as irrespective of the fibre angle. The change in the crack line mainly occurred at the interlace, where the specimen structure showed signs of localised weakening. An example of type C damage is presented in Figure 10.

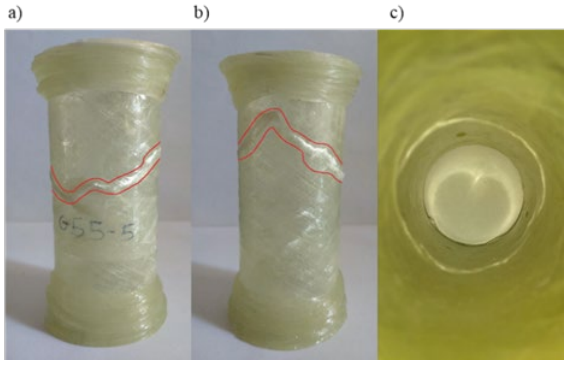

Fig. 10. C type crack in GFRP specimen. Different views of specimen (a and b); internal surface of specimen (c)

Next, the BFRP specimens are described.

L type damage – break along the fibre line – the break in the component followed a similar pattern to type V damage with the exception that the interlace did not result in a change in direction to the opposite angle to the original. This type of damage mostly ran through the entire specimen, at the angle of fibre winding. The structure remained mostly coherent, while localised delamination can be seen along the crack. A crack is shown in Figure 11.

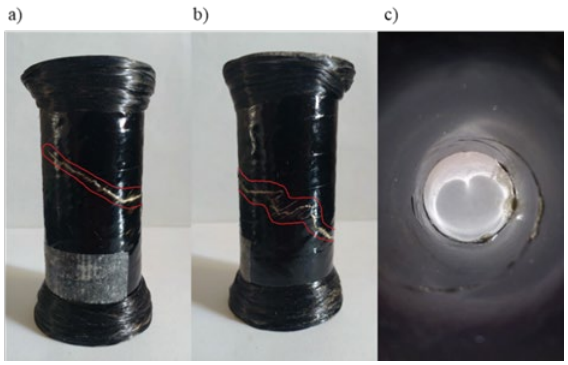

Fig. 11. L type crack in BFRP specimen. Different views of specimen (a and b); internal surface of specimen (c)

LP type damage – crack linearly perpendicular to the axis – the failure pattern of the specimen was not primarily related to the angle at which the fibre was wound on the element. The longest sections of the crack were straight lines perpendicular to the element axis, which may suggest a dominance of shear stresses relative to normal stresses compared to the fibre axis. In some cases, the crack ran through the entire wall thickness and the crack areas were relatively even. The loss of material cohesion can be seen in Figure 12.

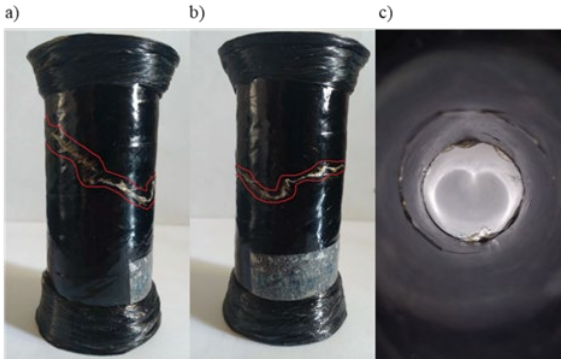

Fig. 12. LP type crack in BFRP specimen. Different views of specimen (a and b); internal surface of specimen (c)

"Elephant foot" type damage – a crack of this type occurred just outside the edge reinforcement area, causing local buckling in part of the specimen. The structure in this area was deformed and fibre delamination was visible in some areas. An example of such damage is illustrated in Figure 13.

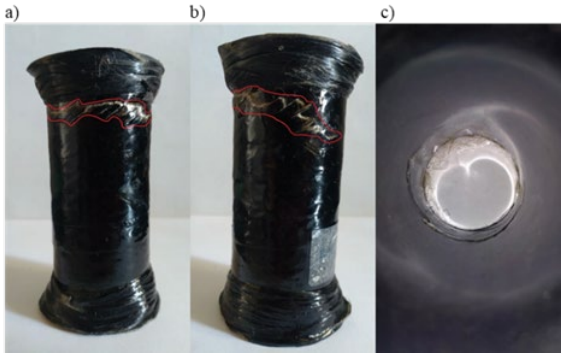

Fig. 13. "Elephant foot" type crack in BFRP specimen. Different views of specimen (a and b); internal surface of specimen (c)

A summary of the crack types occurring in the specimens is presented in Table 3 below.

TABLE 3. **Type of cracks in each specimen**

Specimen	Type of damage
B55-1	LP
B55-2	Elephant foot
B55-3	L
B55-4	L
B55-5	LP
B55-6	L
B55-7	LP
G55-1	C
G55-2	V
G55-3	V
G55-4	C
G55-5	C
G55-6	C
G55-7	V

CONCLUSIONS

In the presented research, filament-wound composite tubes were subjected to axial compression loading. Two types of specimens were analysed: GFRP and BFRP. One layer was wound using a ±55° winding angle. During the axial compression test, the acoustic emission method was utilised to investigate the types of damage modes. Additionally, post-failure observations of cracks were performed.

Based on the conducted study, the following conclusions were drawn:

- The GFRP tubes performed better than BFRP in terms of mechanical parameters, such as compressive strength (41% difference) and corrected energy (20% difference),
- The analysis of the acoustic emission events revealed that for both types the dominant damage was matrix cracking, then delamination/debonding and finally fibre breakage. In terms of the differences, the BFRP specimens exhibited a higher share of M2 compared the GFRP ones, which means that the tubes with basalt fibres were more prone to delamination.
- Macroscopic observations of the specimens after the experiments revealed that in terms of GFRP, the crack propagated more stably and evenly along the winding angle, with the possibility to close the crack along the circumference. In contrast, the BFRP specimens performed less uniformly, with crack direction variations.

Acknowledgement

The presented research results were obtained as part of the research task entitled: "Assessment of the Strength of Composite Pipes under Axial Compression Using Acoustic Emission," financed by a pro-quality subsidy for development of the research potential of the Faculty of Mechanical Engineering of the Wrocław University of Science and Technology in 2024.

REFERENCES

[1] Reddy S.S., Yuvraj C., Rao K.P., Design, Analysis, Fabrication and Testing of CFRP with CNF Composite Cylinder for Space Applications. International Journal of Composite Materials 2015;5:102–28. https://doi.org/10.5923/J.CMATERIALS.20150505.03.

[2] Błażejewski W., Barcikowski M., Stosiak M., Warycha J., Stabla P., Smolnicki M., et al., A novel design of a low-pressure composite vessel with inspection opening – design, manufacturing and testing. Alexandria Engineering Journal 2024;91. https://doi.org/10.1016/j.aej.2024.01.078.

[3] Vasiliev V.V., Composite Pressure Vessels: Analysis, Design, and Manufacturing. Blacksburg, Vir.: Bull Ridge Pub; 2009.

[4] Peters S.T. (Stanley T), Composite filament winding. 1st ed. Materials Park: ASM International; 2011.

[5] Duda S., Lesiuk G., Zielonka P., Stabla P., Flexural Pseudo-Ductility Effect in Hybrid GFRP / CFRP Bars. Materials 2021.

[6] Smolnicki M., Duda S., Zielonka P., Stabla P., Lesiuk G., Lopes C.C.C., Combined experimental–numerical mode I fracture characterization of the pultruded composite bars. Archives of Civil and Mechanical Engineering 2023;23:1–11. https://doi.org/10.1007/S43452-023-00684-W/FIGURES/15.

[7] Smolnicki M., Stabla P., Finite element method analysis of fibre-metal laminates considering different approaches to material model. SN Appl Sci 2019;1. https://doi.org/10.1007/s42452-019-0496-2.

[8] Stabla P., Lubecki M., Smolnicki M., The effect of mosaic pattern and winding angle on radially compressed filament-wound CFRP composite tubes. Compos Struct 2022; 292:115644. https://doi.org/10.1016/j.compstruct.2022.115644.

[9] Orman S., Dogu M., Ozbek B., Optimization of the Filament Winding Process for Glass Fiber-Reinforced PPS and PP Composites Using Box–Behnken Design. Polymers 2024, Vol 16, Page 3488 2024;16:3488. https://doi.org/10.3390/POLYM16243488.

[10] Mertiny P., Juss K., El Ghareeb M.M., Evaluation of glass and basalt fiber reinforcements for polymer composite pressure piping. Journal of Pressure Vessel Technology, Transactions of the ASME 2009;131. https://doi.org/10.1115/1.4000360/444092.

[11] Scalici T., Pitarresi G., Badagliacco D., Fiore V., Valenza A., Mechanical properties of basalt fiber reinforced composites manufactured with different vacuum assisted impregnation techniques. Compos B Eng 2016;104:35–43. https://doi.org/10.1016/J.COMPOSITESB.2016.08.021.

[12] Parmar S., Mankodi H., Basalt Fiber: Newer Fiber for FRP Composites. International Journal of Emerging Technologies in Engineering Research (IJETER) 2016;4.

[13] Yıldızel S.A., Mechanical and thermal behaviors comparison of basalt and glass fibers reinforced concrete with two different fiber length distributions. Challenge Journal of Structural Mechanics 2017;3:155. https://doi.org/10.20528/CJSMEC.2017.12.017.

[14] Manojprabhakar M., Rajini N., Mayandi K., Subash K., Subramanian S., Ramabala Seelan S.V., et al., Impact response of basalt composite pipe using filament winding. J Phys Conf Ser 2019;1240:012104. https://doi.org/10.1088/1742-6596/1240/1/012104.

[15] Fidan S., Özsoy M.İ., Bora M.Ö., Ürgün S., Advanced hybrid composites: A comparative study of glass and basalt fiber reinforcements in erosive environments. Polym Compos 2024;45:12071–91. https://doi.org/10.1002/PC.28619.

[16] Wei B., Cao H., Song S.. Tensile behavior contrast of basalt and glass fibers after chemical treatment. Mater Des 2010;31:4244–50. https://doi.org/10.1016/J.MATDES.2010.04.009.

[17] Hussein E., Acoustic Emission. Non-destructive testing, Chulalongkorn University; 1996, p. 125–44.

[18] Smolnicki M., Duda S., Stabla P., Osiecki T., Mechanical investigation on interlaminar behaviour of inverse FML using acoustic emission and finite element method. Compos Struct 2022;294:115810. https://doi.org/10.1016/J.COMPSTRUCT.2022.115810.

[19] Unnthorsson R., Runarsson T.P., Jonsson M.T., Acoustic emission based fatigue failure criterion for CFRP. Int J Fatigue 2008;30:11–20. https://doi.org/10.1016/J.IJFATIGUE.2007.02.024.

[20] Liao B.B., Wang D.L., Hamdi M., Zheng J.Y., Jiang P., Gu C.H., et al., Acoustic emission-based damage characterization of 70 MPa type IV hydrogen composite pressure vessels during hydraulic tests. Int J Hydrogen Energy 2019;44:22494–506. https://doi.org/10.1016/J.IJHYDENE.2019.02.217.

[21] Saeedifar M., Zarouchas D., Damage characterization of laminated composites using acoustic emission: A review. Compos B Eng 2020;195:108039. https://doi.org/10.1016/J.COMPOSITESB.2020.108039.

[22] Błachut A., Wollmann T., Panek M., Vater M., Kaleta J., Detyna J., et al., Influence of fiber tension during filament winding on the mechanical properties of composite pressure vessels. Compos Struct 2023;304:116337. https://doi.org/10.1016/J.COMPSTRUCT.2022.116337.

[23] Błachut A., Wollmann T., Panek M., Vater M., Kaleta J., Detyna J., et al., Influence of fiber tension during filament winding on the mechanical properties of composite pressure vessels. Compos Struct 2023;304:116337. https://doi.org/10.1016/J.COMPSTRUCT.2022.116337.

[24] Carroll M., Ellyin F., Kujawski D., Chiu A.S., The rate-dependent behaviour of ± 55° filament-wound glass-fibre/epoxy tubes under biaxial loading. Compos Sci Technol 1995;55:391–403. https://doi.org/10.1016/0266-3538(95)00119-0.

[25] Bai J., Seeleuthner P., Bompard P., Mechanical behaviour of ± 55 ° filament-wound glass-fibre/epoxy-resin tubes: I. Microstructural analyses, mechanical behaviour and damage mechanisms of composite tubes under pure tensile loading, pure internal pressure, and combined loading. Compos Sci Technol 1997;57:141–53. https://doi.org/10.1016/S0266-3538(96)00124-8.

[26] Rafiee R., Torabi M.A., Maleki S., Investigating structural failure of a filament-wound composite tube subjected to internal pressure: Experimental and theoretical evaluation. Polym Test 2018;67:322–30. https://doi.org/10.1016/j.polymertesting.2018.03.020.

[27] Azeem M., Ya H.H., Kumar M., Stabla P., Smolnicki M., Gemi L., et al., Application of Filament Winding Technology in Composite Pressure Vessels and Challenges: A Review. J Energy Storage 2022;49:103468. https://doi.org/10.1016/ j.est.2021.103468.

[28] Humberto J., Almeida Júnior J.H., Ribeiro M.L., Tita V., Faria H., Marques A.T., et al., Progressive failure analysis of filament wound composite tubes under internal pressure. 20th International Conference on Composite Materials 2015.

[29] Almeida J.H.S., Ribeiro M.L., Tita V., Amico S.C., Damage and failure in carbon/epoxy filament wound composite tubes under external pressure: Experimental and numerical approaches. Mater Des 2016;96:431–8. https://doi.org/10.1016/j.matdes.2016.02.054.

[30] Jones R.M., Mechanics of Composites Materials. Taylor & Francis Group; 1999.

[31] Vasiliev V.V., Morozov E V. Mechanics and Analysis of Composite Materials. 2001.

[32] Almeida J.H.S., St-Pierre L., Wang Z., Ribeiro M.L., Tita V., Amico S.C., et al., Design, modeling, optimization, manufacturing and testing of variable-angle filament-wound cylinders. Compos B Eng 2021;225:109224. https://doi.org/10.1016/j.compositesb.2021.109224.

[33] Wadim J., Acoustic emission applications. San Juan Capistrano 1978.

[34] Kotsikos G., Evans J.T., Gibson A.G., Hale J., Use of acoustic emission to characterize corrosion fatigue damage accumulation in glass fiber reinforced polyester laminates. Polym Compos 1999;20:689–96. https://doi.org/10.1002/PC.10392.

[35] Gong L., Nouvells approche de l'emission acoustique et son application a l'identification des mecanismes d'endommagement dans les materiaux composites. Revue Des Composites et Des Materiaux Composites Avancees 1998;8:7–23. Zhang J., Zhang R., Geerlings H., Bi J., (2010). A novel indirect wollastonite carbonation route for CO2 sequestration. Chemical Engineering and Technology, 33(7), 1177-1183.